11th ANKARA INTERNATIONAL AEROSPACE CONFERENCE **AIAC-2021-059**
8-10 September 2021 - METU, Ankara TURKEY

MODELING OF THE HAWKMOTH WING AND ITS IMPLEMENTATION IN A FLAPPING WING MECHANISM

Aytek Altuga Ökmen[1] Asst.Prof.Dr.Kutluk Bilge Arıkan[2] Prof. Dr. Dilek Funda Kurtuluş[3]
METU TED University METU
Ankara, Turkey Ankara, Turkey Ankara, Turkey

ABSTRACT

Main aim of this study is to accurately model the wing of a hawkmoth (Manduca sexta) in order to implement it in a flapping wing mechanism for a micro aerial vehicle (MAV). The wing is first modeled in ANSYS/SpaceClaim then the model is verified by performing modal analysis on the finite element model (FEM) of the wing in ANSYS/Mechanical. Grid refinement study is performed on the FEM. Results of the modal analysis of the modeled wing is compared to literature results and it is seen that both results are in good agreement. A simple planar four bar mechanism is designed in flexible multibody dynamics program ADAMS. The mechanism can perform a figure of eight shape when it is moving which mimics the flapping motion of hawkmoth. It is planned that the flapping mechanism will be further improved and optimized according to the initial simulation results.

INTRODUCTION

The importance of micro aerial vehicles (MAVs) is increasing rapidly day by day. They have vast usage areas such as but not limited to surveillance, search-rescue and entertainment. There are three kinds of MAVs which are fixed wing, rotary wing and flapping wing. While fixed wing MAVs have extended ranges their maneuverability is limited and they cannot hover whereas the rotary wing MAVs have the other way around. Focus is developing advanced flapping wing MAVs (FWMAVs) which offer greater maneuverability than fixed wing MAVs and longer ranges than rotary wing MAVs which can also hover. Besides having significant advantages than both fixed and rotary wing MAVs, FWMAVs are the hardest to model, design and manufacture.

A literature survey is conducted about the unsteady flapping aerodynamics, morphology of the hawkmoth wing as well as flapping wing mechanisms. Unsteady flapping aerodynamics is previously researched extensively by Kurtulus et al. (2004, 2005, 2006a-c, 2008), Kurtulus (2009,2011), Akay et al. (2007) both numerically and experimentally. Two different theses are examined carefully for understanding the wing morphology of the hawkmoth. In the first study, effects of wing venation are shown as well as constant camber. Thickness of the wing is given as 0.12 mm. The modeled wing has a root chord instead of a single attachment point between the abdomen of the hawkmoth and its wing. Modal analysis is performed on the modeled wing both with and without the veins as well as finding the natural frequency of a flat paper wing [Sims, 2010]. In the second study, the modeled wing attaches to the insect's body through a single point and it has a variable camber throughout the span of the wing. At the wing root, camber shape is concave down with maximum distance of 1 mm. and at the wing tip the

[1] M.Sc. Student in Department of Aerospace Engineering, Email: okmen.altuga@gmail.com
[2] Prof. in Department of Mechnical Engineering, Email: kutluk.arikan@tedu.edu.tr
[3] Prof. in Department of Aerospace Engineering, Email: funda.kurtulus@ae.metu.edu.tr

camber is concave up with a maximum distance of 1 mm again. Span of the wing is 50 mm. Transition to concave down to concave up camber occurs approximately at 52% of the span. Veins are also taken into account like in Sims (2010) model [O'Hara, 2012].

Wing model of O'Hara (2012) is chosen for verifying the designed model since it represents the real hawkmoth wing better with a single point at the root chord.

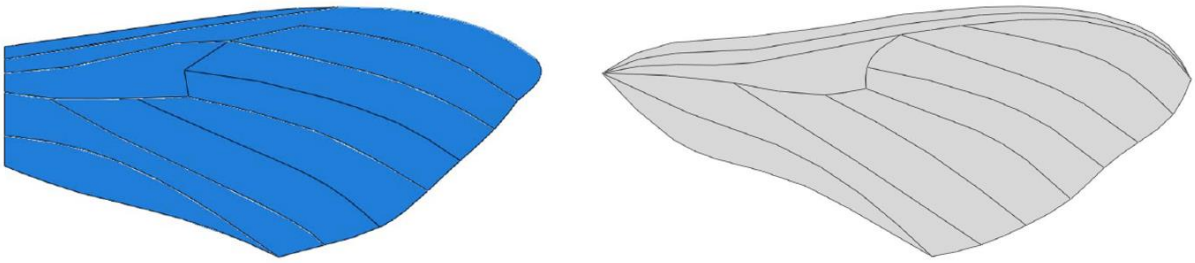

(a) (b)

Figure 1: (a) Wing model of Sims (2010) (b) Wing model of O'Hara (2012)

Lemniscate mechanism is selected from a list of different mechanisms [Artobolevsky, 1976]. It is kind of a four-bar mechanism which can perform plunging and pitching motions of the wing when flapping. It is also seen that torsion springs are used for pitching motion [Khan, Agrawal, 2007]. Another study shows bearings are used in a study for making the flapping wings perform pitching [Burgess, Alemzadeh, Zhang, 2004]. All of these pitching methods are considered passive since no electronic controller is present. A spherical flapping mechanism which is inspired from the human shoulder joint is investigated as well [Rehmat et al., 2009]. In this spherical flapping mechanism no pitching is performed by the wing. In some study it is seen that materials like carbon fiber are used for increased endurance [Nguyen, Chan, Debiasi, 2014]. With the help of another study, the simplicity and effectiveness of the planar four bar mechanisms are understood [Zbikowski et al., 2004]. A mechanism uses pulleys in order to mimic the broad stroke amplitude when insects and some birds are hovering. And with the help of flexible materials wing can twist and bend [Phan et al., 2016]. Finally, a double scotch yoke mechanism is used for flapping. Main aspect of this study is to achieve a smoother flapping movement and reduce overall stress over mechanism parts. As a result, aerodynamic forces and loads become more dominant [Zbikowski, Galinsky, 2005].

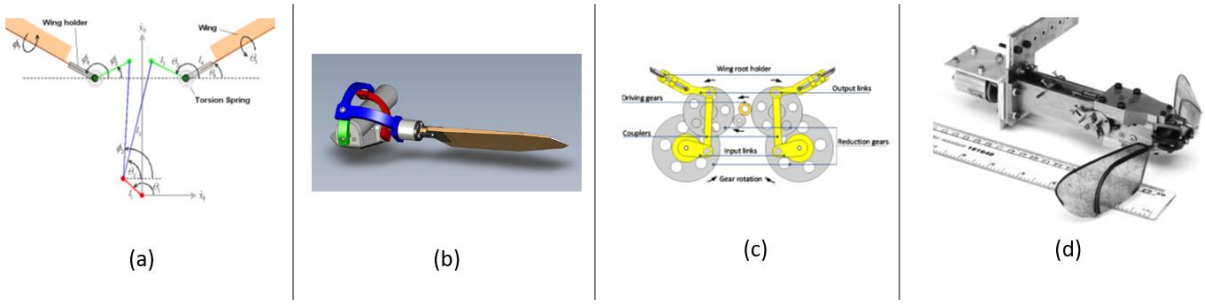

(a) (b) (c) (d)

Figure 2: (a) Mechanism of Khan, Agrawal (2007) (b) Mechanism of Rehmat et al. (2009) (c) Mechanism of Nguyen et al. (2014) (d) Mechanism of Zbikowski, Galinsky (2005)

METHOD

The wing modeling is done with ANSYS/SpaceClaim. Second part is performing the wing model's modal analysis for model verification and grid refinement. Third part is designing the mechanism and modeling it in ADAMS.

Wing Model

First the outer shape and veins of the wing is drawn in CAD program SpaceClaim. The wing drawing and vein names can be seen in Figure 3. Vein names are taken from O'Hara (2012).

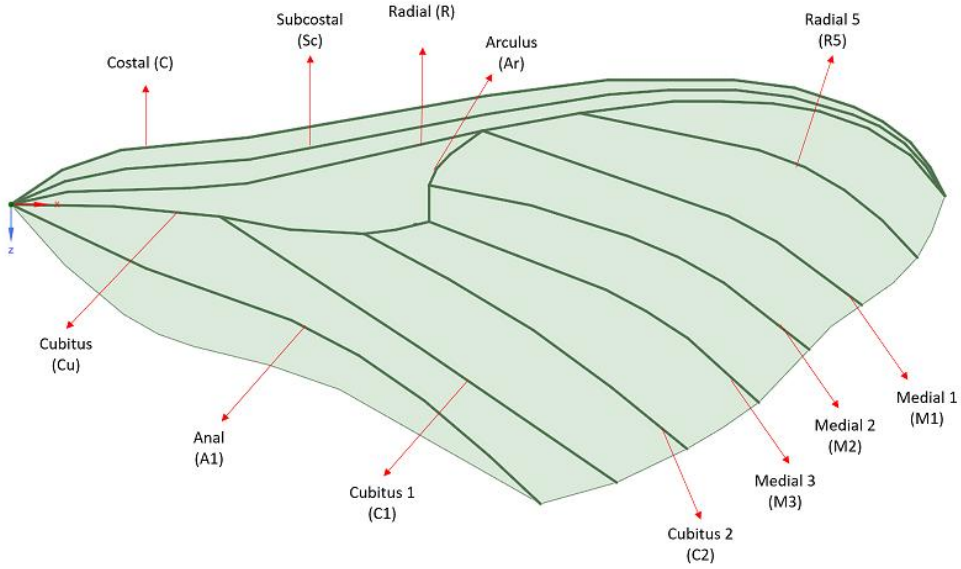

Figure 3: Vein Nomenclature of the Hawkmoth Wing

Span of the wing is 50 mm. and the maximum chord is 23 mm. The origin of the wing root has a perpendicular distance of 7 mm from the maximum point of the leading edge. It has a complex camber shape. At the wing root (origin point), camber is shaped concave down with a maximum distance of 1mm. At the wing tip, camber is shaped concave up with a maximum distance of 1 mm. Transition from concave down to concave up occurs at approximately 50% distance in the spanwise direction.

Veins of the wing are modeled as circular tubes (BEAM188) and the membrane is modeled as a shell (SHELL181) with a thickness of 5 μm. Inner diameters of the veins are approximately 70% of the outer vein diameters. The tip and root diameters of the veins can be seen in the table below.

Table 1: Vein Names and Diameters

Vein Name	Root Diameter (μm)	Tip Diameter (μm)
Costal	250	20
Subcostal	250	20
Radial	250	20
Cubitus	250	130
Arculus	130	70
Radial 5	130	20
Medial 1	130	20
Medial 2	130	20
Medial 3	130	20
Cubitus 1	150	20
Cubitus 2	150	20
Anal	150	20

Modal Analysis

Modal analysis is performed on the modeled wing with different mesh sizes. A grid refinement study is conducted. Grid sizes are chosen as 0.3 mm for fine mesh, 0.4 mm for medium size and 0.5 mm for coarse mesh. Properties of wing models with different mesh element sizes are

specified along with O'Hara (2012) specifications in Table 2. The bounding box of the wing model is (50.39, 2.3, 23) mm in (x, y, z) directions respectively. First natural frequencies and mode shape results of the chosen mesh sizes are compared with the result of O'Hara (2012) in Table 3.

Table 2: Properties of Wings with Different Element Size

Element Size	**0.3 mm**	**0.4 mm**	**0.5 mm**	**O'Hara (2012)**
Mass (kg)	2.74e-5	2.74e-5	2.74e-5	2.86e-5
Moment of Inertia (x-axis)	1.28e-10 kg.m^2	1.28e-10 kg.m^2	1.28e-10 kg.m^2	2.99e-10 kg.m^2
Moment of Inertia (y-axis)	7.92e-10 kg.m^2	7.92e-10 kg.m^2	7.92e-10 kg.m^2	1.14e-8 kg.m^2
Moment of Inertia (z-axis)	6.64e-10 kg.m^2	6.64e-10 kg.m^2	6.64e-10 kg.m^2	1.16e-8 kg.m^2
Centroid(X, Y, Z mm)	(26.98, -4.5e-2, 2.9)	(26.98, -4.5e-2, 2.9)	(26.98, -4.5e-2, 2.9)	(22.1, 4.0, 0)
Nodes	10251	5986	3407	-
Elements	10100	5879	3333	-

From Table 2, it is seen that the masses and moments of inertia of two different models are almost identical and the differences are negligible further proving the accuracy of the constructed model with the existing literature.

Table 3: Natural Frequencies

Element Size (mm)	**Natural Frequency (Hz)**
0.3	64.946
0.4	65.056
0.5	65.212
O'Hara (2012) Model	65.200
O'Hara (2012) Experimental Data	65

From Table 3, it can be deduced that the medium sized mesh with 0.4 mm element size is in good agreement with the experimental data of 65 Hz. and within a very small margin to numerical data of 65.2 Hz. both obtained by O'Hara (2012). Although coarse mesh (0.5 mm element size) is almost identical to numerical value of O'Hara (2012), it is seen that medium sized mesh's results is closer to the experimental results which implies the model represents an actual wing more accurately. Mode shape results of all meshes in comparison with the O'Hara (2012) mode shape result can be seen in Figure 4.

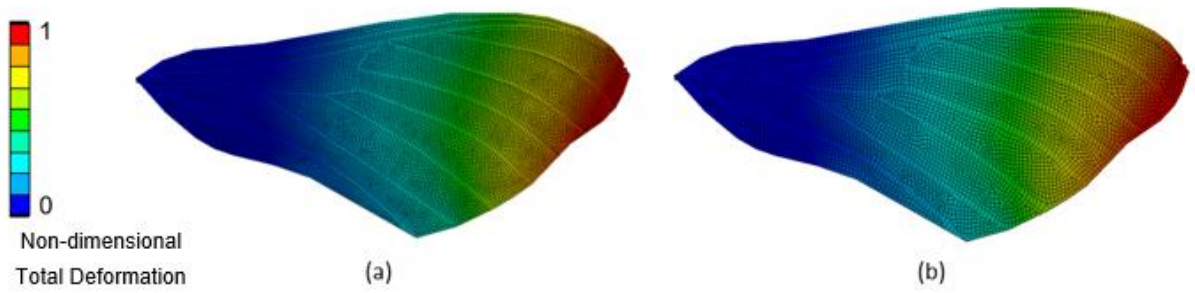

(a) 0.3 mm Element Size FEA Model (b) 0.4 mm Element Size FEA Model

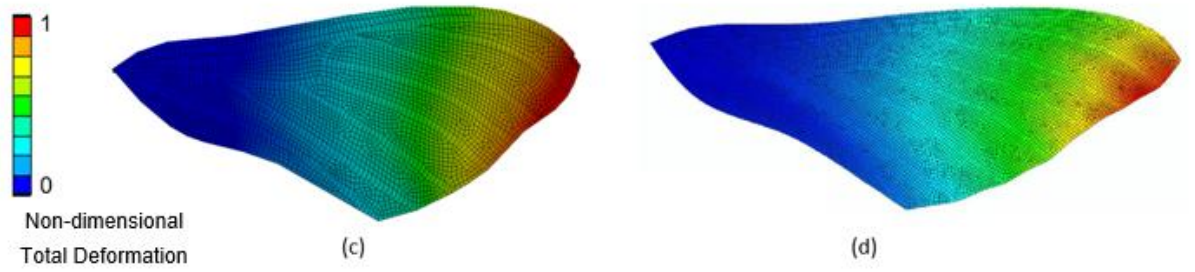

(c) 0.5 mm Element Size FEA Model (d) FEA Wing Model of O'Hara [2012]

Figure 4: Mode shapes of different meshes on the modeled wing in comparison with literature data

From Figure 4, it is obvious that constructed model's mode shapes are in good agreement with the results of the model chosen from the literature [O'Hara, 2012]. The contours in Figure 4, represent the non-dimensional total deformation, non-dimensionalized with respect to the maximum deflection at the tip of the wing.

Effect of different inner vein diameter to outer vein diameter ratio is also examined by performing two different modal analyses with inner vein diameters of 60% and 80% outer vein diameters instead of previously used 70%. Both models are solved with an element size of 0.4 mm. Numerical results can be seen in Table 4 and mode shape results can be seen in figure 5. From Table 4, it is seen that there is negligible difference between the first bending mode for different vein diameter ratios. However, they differ from the previously used ratio and it is seen that in order to preserve the accuracy of the model inner vein diameters should be 70% of the outer vein diameters. It can also be said that as vein diameter ratio gets smaller mass of the model increases because veins get thicker overall.

Table 4: Numerical Results for Different Vein Diameter Ratios

Vein Diameter Ratio	60%	80%
First Natural Frequency (Hz)	70.804	70.828
Mass (kg)	3.82e-5	2.40e-5

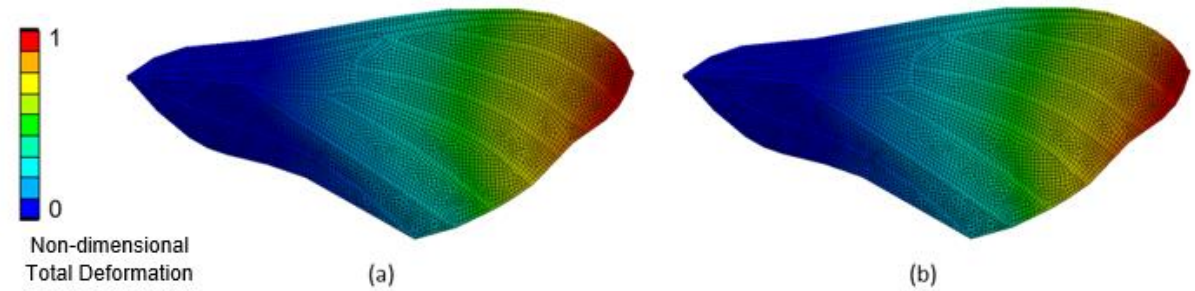

Figure 5: Mode Shapes of Wings with (a) 60% Inner Vein Diameter (b) 80% Inner Vein Diameter

Material Study

Previously constructed wing model is modified for observing its natural frequency when its material is changed. The organic materials defined previously and newly chosen composite materials are shown in below table 5.

Table 5: Properties of Materials

Material	Organic		Composite	
	Vein	Membrane	Carbon Fiber	Mylar
Density (kg/m^3)	2452	1400	1600	1250
Young's Modulus (GPa)	7.41	2.4	70	7
Poisson's Ratio	0.3	0.3	0.1	0.25

Values for carbon fiber are taken from Truong et al. (2017) and values for mylar are taken from Singh & Chopra (2008). For organic materials values from O'Hara (2012) are used. Three different models are used. First model is flat (no camber) and has no veins, second model is cambered but without veins and final model is both cambered and has veins. Mylar is only used in the third model as membrane whereas other two models are entirely carbon fiber. Element size of 0.4 mm is used in modal analysis for all three models. First natural frequency (bending mode) of the flat carbon fiber wing without veins is found as 0.995 Hz. Natural frequency of the second model with camber but no veins is found as 1.345 Hz. which shows that the effect of camber is rather small. However, cambered and veined third model's results yielded 227.21 Hz. This great increase is mainly caused by the addition of carbon fiber veins which add tremendous strength as a result of carbon fiber's high Young's modulus.

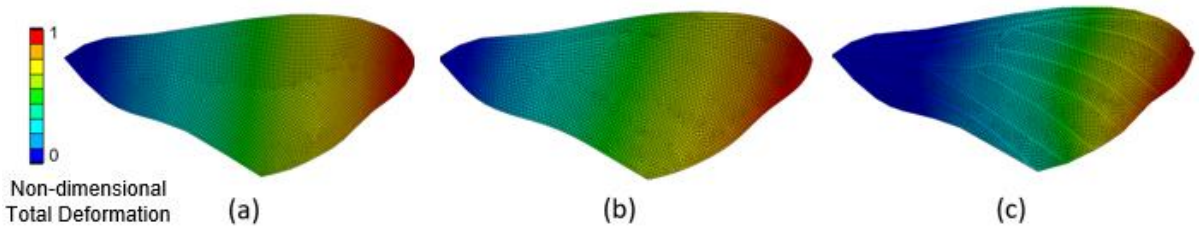

Figure 6: Mode Shape Results of Carbon Fiber Wings (a) without Camber and without Veins (b) with Camber and without Veins (c) with Camber and with Veins

Mechanism

A flapping wing which can perform pitching and plunging motion is modeled in flexible multibody dynamics program ADAMS. Lemniscate mechanism of Artobolevsky (1976), is chosen for flapping mechanism. The simple mathematical model of the mechanism is given in equation 1.

$$(x^2 + y^2) = a^2(x^2 - y^2) - 4b^2y^2 \quad (1)$$

In equation 1, x and y are the coordinates and a and b are link lengths. Long link and the distance between short links is 2b and the length of the short links are a. In order for the mechanism to be able to draw the figure of eight shape, the condition $a = \sqrt{2b}$ must be satisfied.

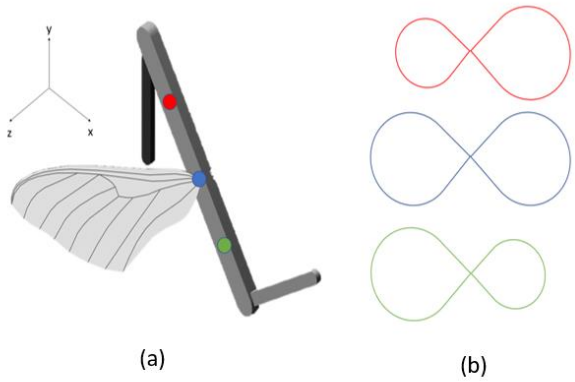

(a) (b)

Figure 7: (a) Wing Locations on the Mechanism (b) Figure of eight motion According to Wing Placement

In Figure 5, the flapping mechanism with the constructed wing model attached can be seen. Mechanism is driven from the short link at the front (-x direction). Wing is placed at the locations denoted by red, blue and green dots with its tip facing the +z direction. Figure 7b shows how the figure of eight shape is changed according to the wing placement on the mechanism. When the wing is placed at the red dot, the figure of eight's front loop is smaller than the rear. When the wing is placed at the green dot, figure of eight's rear loop is smaller than the front. Finally, if the wing is placed at the blue dot (middle point of the long link as well as its center of mass) both sides of the figure of eight shape is equal. This enables for obtaining numerical lift data from different places on the mechanism and optimize it accordingly. Long link rotates around its middle point while short links of the mechanism are rotating in opposite directions thus performing a passive pitching motion. At the same time, tip of the wing is drawing an 8 shape corresponding to its place on the long link.

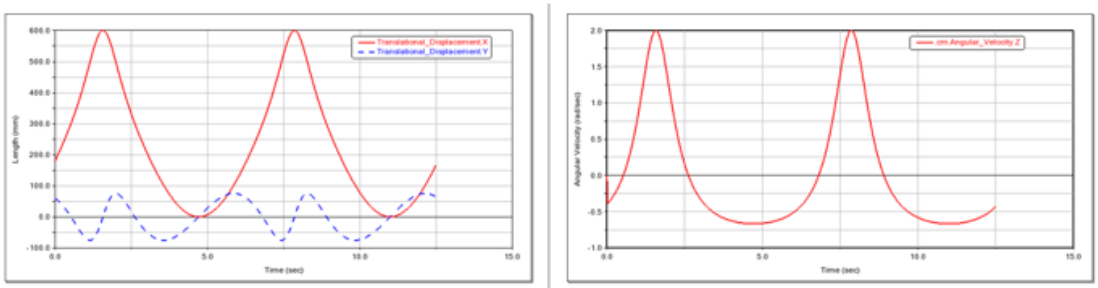

(a) (b)

Figure 8: (a) Displacement of the Wing Attachment Point in x-axis (red line) and y-axis (dashed blue line) (b) Angular Velocity of the Wing Attachment Point Around z-axis when the Wing is Attached to Middle (Blue) Point

Figure 8a depicts that the long link of the mechanism, which the wing is attached, is performing plunging motion by showing translational displacement in x direction (red line) and in y direction (dashed blue line). Figure 8b depicts that there is an angular velocity around z-axis. This shows while the mechanism is in motion, long link rotates around its center of mass (middle point) which means the wing is pitching.

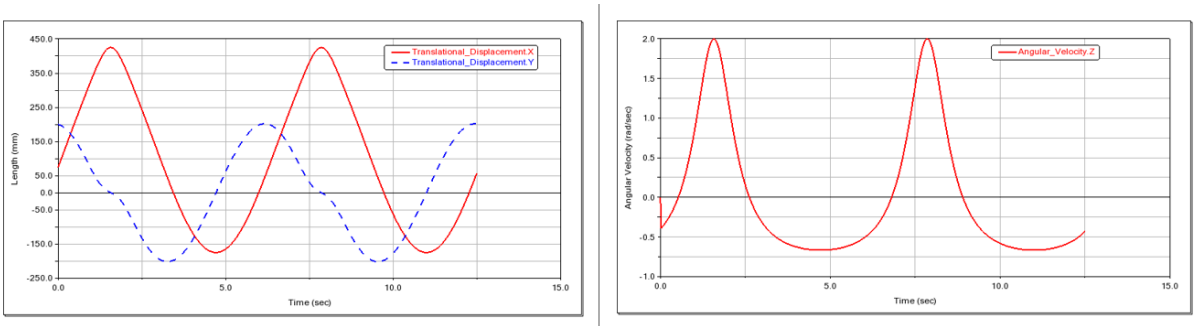

(a) (b)

Figure 9: (a) Displacement of the Wing Attachment Point in x-axis (red line) and y-axis (dashed blue line) (b) Angular Velocity of the Wing Attachment Point Around z-axis when the Wing is Attached to Front (Red) Point

In Figure 9a, translational displacement in x and y direction are shown with red and dashed blue lines again respectively. In Figure 9b, angular velocity around z-axis is shown. However, in Figure 9 the wing is attached to the mechanism at the front (red point shown in Figure7a) instead of middle point (shown in Figure 8). It is seen that the displacement in y direction is increased at the front point when compared to middle point while the angular velocity remains unchanged between two points. This indicates that plunging motion is stronger at the red point than at the middle point.

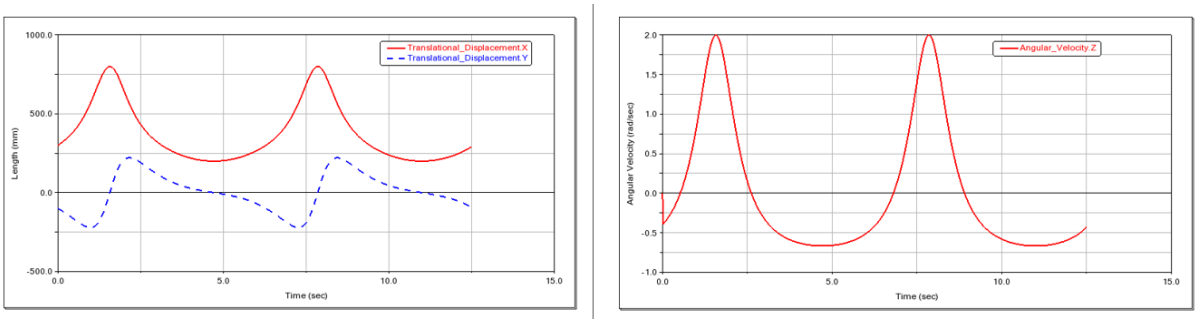

(a) (b)

Figure 10: (a) Displacement of the Wing Attachment Point in x-axis (red line) and y-axis (dashed blue line) (b) Angular Velocity of the Wing Attachment Point Around z-axis when the Wing is Attached to Rear (Green) Point

In similar fashion, Figure 10 shows the translational displacement in x-axis and y-axis as well as angular velocity around z-axis. Again, the angular velocity is same with other two points. However, translational displacement is even further increased when compared against other two points in both x and y directions. The duration for all three simulations is 12 seconds and it is considered that wing is in a vacuum, meaning no aerodynamic effects are considered and obtained data is purely inertial.

DISCUSSION AND CONCLUSION

The main aim of this study is to design, simulate and optimize a flapping wing mechanism. Wing of hawkmoth (Manduca sexta) is chosen to be used since it has been studied thoroughly and there is vast knowledge about its morphological characteristics.
First a brief literature survey is conducted about flapping wing mechanisms and the biological properties of hawkmoth wing. After that, the wing is modeled as a flexible finite element model. The accuracy of the constructed model is verified by performing a modal analysis in order to find its natural frequency and compare it to the data present in the literature.
After the wing model is verified, a planar, four-bar lemniscate mechanism is designed which can mimic the pitching and plunging of the wing by drawing a figure of eight shape with the wingtip. Three distinct locations are chosen on the long link and three simulations are run. Obtained data from different locations are compared with each other, providing an insight about the optimum wing attachment location. Modularity of the mechanism is achieved through the availability of different wing placement locations along the long link of the mechanism. This allows gathering extensive numerical lift force data from numerous different locations along the link and choosing the location where the optimal lift force is generated by the wing.

ACKNOWLEDGEMENT

This work is supported by TUBITAK 116M273 project.

References

Artobolevsky, I. I. (1976). Mechanisms in Modern Engineering Design. MIR.

Akay B, Kurtulus D.F., Alemdaroglu N (2007) Unsteady Aerodynamics of Different Wing Profiles at Low Reynolds Number. RTO-MP-AVT-146, NATO AVT-146 Symposium on Platform Innovations and System Integration for Unmanned Air, Land and Sea Vehicles, 14-17 May 2007, Florence, Italy.

Burgess, S. C., Alemzadeh K., Zhang, L., 2004. “The Development of a Miniature Mechanism for Producing Insect Wing Motion”, Design and Nature II pp. 237-248

Khan, Z., A., Agrawal, S., K., 2007. “Design and Optimization of a Biologically Inspired Flapping Mechanism for Flapping Wing Micro Air Vehicles”, IEEE International Conference on Robotics and Automation, 373-378.

Kurtulus D.F. (2009) Ability to forecast unsteady aerodynamic forces of flapping airfoils by Artificial Neural Network, Neural Computing & Applications, Vol. 18, Issue 4, pp.359-368.

Kurtulus D.F., David L, Farcy A, Alemdaroglu N (2008) Aerodynamic Characteristics of Flapping Motion in Hover. Experiments in Fluids, Vol. 44, pp. 23–36.

Kurtulus D.F. (2011) Introduction to micro air vehicles: concepts, design and applications, VKI LS 2011-04, Recent developments in unmanned aircraft systems, (UAS, including UAV and MAV), Ed. Carbonaro M., Decuypere R., ISBN-13 978-2-87516-017-1, April 2011, pp. 219-255.

Kurtulus D.F., David L, Farcy A, Alemdaroglu N (2006a) Aerodynamic Characteristics of Flapping Motion in Hover. 13th Int Symp on Applications of Laser Techniques to Fluid Mechanics, 1130, Lisbon, Portugal, 26-29 June 2006

Kurtulus DF, David L, Farcy A, Alemdaroglu N (2006b) A Parametrical Study with Laser Sheet Visualization for an Unsteady Flapping Motion. AIAA-2006-3917, 36th AIAA Fluid Dynamics Conference and Exhibit, San Francisco, California USA, 5 - 8 June 2006.

Kurtulus D.F., David L, Farcy A, Alemdaroglu N (2006c) Laser Sheet Visualization for Flapping Motion in Hover. AIAA-2006-0254, 44rd AIAA Aerospace Sciences Meeting and Exhibit, Reno, Nevada, USA, 9 - 12 Jan 2006.

Kurtulus D.F., Farcy A, Alemdaroglu N (2005) Unsteady Aerodynamics of Flapping Airfoil in Hovering Flight at Low Reynolds Numbers. AIAA-2005-1356, 43rd AIAA Aerospace Sciences Meeting and Exhibit, Reno, Nevada, USA, 10 - 13 Jan 2005.

Kurtulus D.F., Farcy A, Alemdaroglu N (2004) Numerical Calculation and Analytical Modelization of Flapping Motion. Proceeding of 1st European Micro Air Vehicle Conference and Flight Competition. Braunschweig, Germany, 13-14 July 2004

Nguyen, Q., V., Chan, W., L., Debiasi, M., 2014. “Design, Fabrication, and Performance Test of a Hovering-Based Flapping-Wing Micro Air Vehicle Capable of Sustained and Controlled Flight”, 2014 International Micro Air Vehicle Conference and Competition, IMAV 2014, 18-24.

O’Hara, Ryan, P., The Characterization of Material Properties and Structural Dynamics of the Manduca Sexta Forewing for Application to Flapping Wing Micro Air Vehicle Design. Master's thesis, Air Force Institute of Technology, September 2012.

Phan H., V., Au, T., K., L., Park, H., C., 2016. “Clap and Fling Mechanism in a Hovering Insect-Like Two-Winged Flapping-Wing Micro Air Vehicle”, Royal Society Open Science Volume 3 Issue 12.

Rehmat, Z., Lee, J. S., Roll, J., Yim, W., Trabia, M., B., 2009. “Design of “Figure-8” Spherical Motion Flapping Wing for Miniature UAV”, Proceedings of the ASME 2009 International Design Engineering Technical Conferences & Computers and Information in Engineering Conference, August 30-September 2 2009, San Diego, California, 2009

Sims, T. A Structural Dynamic Anaysis of a Manduca Sexta Forewing. Master's thesis, Air Force Institute of Technology, Wright-Patterson AFB, OH, March

2010. AFIT/GAE/ENY/10-M22.

Singh, B., & Chopra, I. (2008). “Insect-Based Hover-Capable Flapping Wings for Micro Air Vehicles: Experiments and Analysis.” AIAA Journal, 46(9), 2115–2135. doi:10.2514/1.28192

Truong, T. V., Nguyen, Q.-V., & Lee, H. (2017). “Bio-Inspired Flexible Flapping Wings with Elastic Deformation.”, Aerospace*, 4(3), 37.* doi:10.3390/aerospace4030037

Zbikowski, R., Galinski, C., 2005. “Insect-Like Flapping Wing Mechanism Based on a Double Spherical Scotch Yoke”, Journal of Royal Society Interface Volume 2 Issue 3, 223-235.

Zbikowski, R., Knowles, K., Pedersen, C., B., Galinski C., 2004. “Some aeromechanical aspects of insect-like flapping wings in hover”. Proceedings of the Institution of Mechanical Engineers, Part G: Journal of Aerospace Engineering Vol. 218 Issue 6